



## **Influence of carbonate-based additives on the electrochemical performance of Si NW anodes cycled in an ionic liquid electrolyte.**

Killian Stokes, TADHG KENNEDY, Guk-Tae Kim, HUGH GEANEY, Dylan Storan, Fathima R. Laffir, Giovanni Battista Appetecchi, Stefano Passerini, KEVIN M. RYAN

### **Publication date**

01-01-2020

### **Published in**

Nano Letters;20 (10), pp. 7011-7019

### **Licence**

This work is made available under the [CC BY-NC-SA 1.0](#) licence and should only be used in accordance with that licence. For more information on the specific terms, consult the repository record for this item.

### **Document Version**

1

### **Citation for this work (HarvardUL)**

Stokes, K., KENNEDY, T., Kim, G.-T., GEANEY, H., Storan, D., Laffir, F.R., Appetecchi, G.B., Passerini, S. and RYAN, K.M. (2020) 'Influence of carbonate-based additives on the electrochemical performance of Si NW anodes cycled in an ionic liquid electrolyte.', available: <https://hdl.handle.net/10344/9361> [accessed 23 Jul 2022].

This work was downloaded from the University of Limerick research repository.

For more information on this work, the University of Limerick research repository or to report an issue, you can contact the repository administrators at [ir@ul.ie](mailto:ir@ul.ie). If you feel that this work breaches copyright, please provide details and we will remove access to the work immediately while we investigate your claim.

# Influence of Carbonate-Based Additives on the Electrochemical Performance of Si NW Anodes Cycled in an Ionic Liquid Electrolyte

Killian Stokes,<sup>a,b</sup> Tadhg Kennedy,<sup>\*,a,b</sup> Guk-Tae Kim,<sup>c,d</sup> Hugh Geaney,<sup>a,b</sup> Dylan Storan,<sup>a,b</sup> Fathima Laffir,<sup>b</sup> Giovanni Battista Appetecchi,<sup>e</sup> Stefano Passerini,<sup>c,d</sup> and Kevin M. Ryan<sup>\*,a,b</sup>

<sup>a</sup>Department of Chemical Sciences, University of Limerick, V94T9PX, Limerick, Ireland

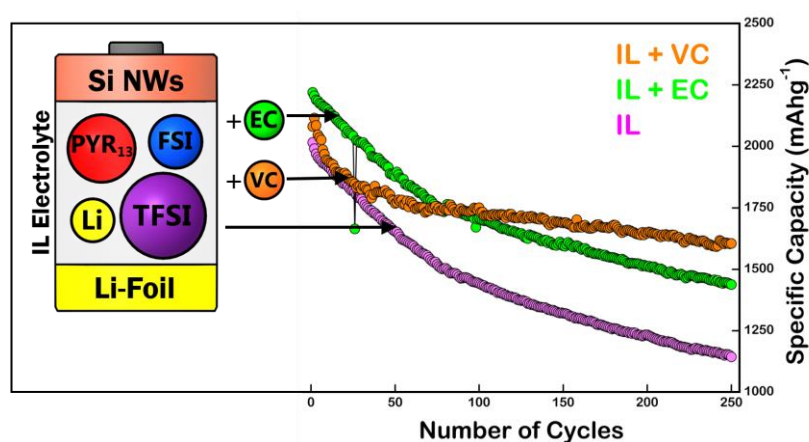
<sup>b</sup>Bernal Institute, University of Limerick, V94T9PX, Limerick, Ireland

<sup>c</sup>Helmholtz Institute Ulm, Karlsruhe Institute of Technology, Helmholtzstrasse 11, 89081 Ulm, Germany

<sup>d</sup>Karlsruhe Institute of Technology, P.O. Box 3640, 76021 Karlsruhe, Germany

<sup>e</sup>ENEA, Italian National Agency for New Technology, Energy and Sustainable Economic Development, Materials and Physicochemical Processes Laboratory, Via Anguillrese 301, 00123 Rome, Italy

## TOC



## Abstract

Addition of electrolyte additives (ethylene or vinylene carbonate) is shown to dramatically improve the cycling stability and capacity retention (1600 mAhg<sup>-1</sup>) of Si nanowires (NWs) in a safe ionic liquid (IL) electrolyte (0.1LiTFSI-0.6PYR<sub>13</sub>FSI-0.3PYR<sub>13</sub>TFSI). We show using post-mortem SEM and TEM, a distinct difference in morphologies of the active material after cycling in the presence or absence of the additives. The difference in performance is shown by

post-mortem XPS analysis to arise from a notable increase in irreversible silicate formation in the absence of the carbonate additives. The composition of the solid electrolyte interphase (SEI) formed at the active material surface was further analysed using XPS as a function of the IL components revealing that the SEI was primarily made up of N, F and S containing compounds from the degradation of the TFSI and FSI anions.

**Keywords:** *Ionic Liquid, Electrolyte, Silicon Nanowires, SEI, Ex-situ*

## **Introduction**

Replacing graphite anodes in Li-ion batteries with Si offers a ten- fold increase in lithium storage capacity, owing to a change from intercalation to alloying as the charge storage mechanism.<sup>1-4</sup> The associated volume changes in alloying (~300% e.g Si) has long meant a negligible cycle life for large particles although significant promise has emerged with nanostructured morphologies to withstand repeated cycling.<sup>5-8</sup> NW morphologies are particularly promising as they can be grown directly from the current collector, offering additional benefits in terms of short Li diffusion distances, good conductivity and the ability to eliminate non-Li active weight from battery (i.e. binders and conductive additives). As a result, binder-free NW based anodes have exhibited some of the best reported cycling stability to date in the literature.<sup>9-13</sup> Initially, the ability of the NWs to survive repeated cycling was thought to be due to the ability of each NW to withstand the volume change, however, recent work has shown that the NWs undergo a morphological evolution from discrete structures into a fibrous porous network that is more resilient.<sup>9, 14</sup> A major remaining hurdle is the instability of the solid electrolyte interphase (SEI) over extended charge/discharge cycles for Si anodes.<sup>15-16</sup> The repeated volume changes during alloying/dealloying fractures the SEI- continually re-exposing the active material each cycle. The SEI is thus under constant repair, resulting in a consequential consumption of the electrolyte and cycleable Li, along with irreversible reactions

with the anode material (e.g. formation of lithium silicates).<sup>17-22</sup> The outcome is a reduced coulombic efficiency and steady/continued fade in capacity.<sup>23-24</sup> The use of electrolyte additives has been investigated to try to overcome these issues, where ‘stable SEI formers’ have been used to form conductive and mechanically flexible SEIs. While additives typically make up just 1–5 wt.% of the electrolyte, they can significantly influence the battery’s electrochemical performance.<sup>14, 25-30</sup>

Currently, most electrolytes employed are volatile and carbonate-based, which can compromise the safety of the battery, with overheating or short-circuiting of the cell leading to thermal runaway and subsequent fire and/or explosion.<sup>31</sup> These safety concerns have prompted research into ionic liquids (ILs) as battery electrolytes due to their low vapour pressure induced inflammability.<sup>32-33</sup> ILs, are room temperature molten salts composed of organic cations paired with inorganic or organic anions. A typical IL electrolyte for a Li-ion battery is based on N-alkyl-N-methylpyrrolidinium cations ((PYR<sub>n</sub>)<sup>+</sup>) with bis-(trifluoromethanesulfonyl)imide (TFSI<sup>-</sup>) or bis-(fluorosulfonyl)imide (FSI<sup>-</sup>) anions.<sup>33-36</sup> Both anions are beneficial to the electrolyte where FSI<sup>-</sup> has moderate viscosity, a low melting point and offers fast ion transport, whereas TFSI<sup>-</sup> possesses a wide electrochemical and thermal stability.<sup>34, 37</sup> Previous reports have confirmed the fundamental compatibility of IL electrolytes with Si and Ge anodes, leading to encouraging electrochemical performance.<sup>38-43</sup> However, despite their key role in determining long term cycling stability, there has been limited research on use of electrolyte additives to improve the performance of Si anodes within IL electrolytes.

In this study, the positive effects of the addition of SEI forming additives (EC and VC) on the performance of Si NWs anodes in a 0.1LiTFSI-0.6PYR<sub>13</sub>FSI-0.3PYR<sub>13</sub>TFSI IL electrolyte are investigated and explained. The base IL electrolyte used combines FSI<sup>-</sup> and TFSI<sup>-</sup> ions in order to access the combination of properties such as wide electrochemical window, good chemical and thermal stability, flame retardancy and negligible vapour

pressures.<sup>44-47</sup> It is shown that the SEI composition and morphological evolution of the active material within the base IL electrolyte are markedly different to the additive containing electrolytes. The incorporation of electrolyte additives not only leads to significant morphological changes of the Si NW arrays during cycling (formation of a connected active material network versus textured NW formation) but also leads to crucial SEI composition differences (specifically a suppression of parasitic Li silicate formation). These factors explain the enhanced electrochemical performance of the electrolyte additive-containing IL and highlight the critical role played by IL electrolyte formulation for high capacity Li-ion anode materials.

## Results & Discussion

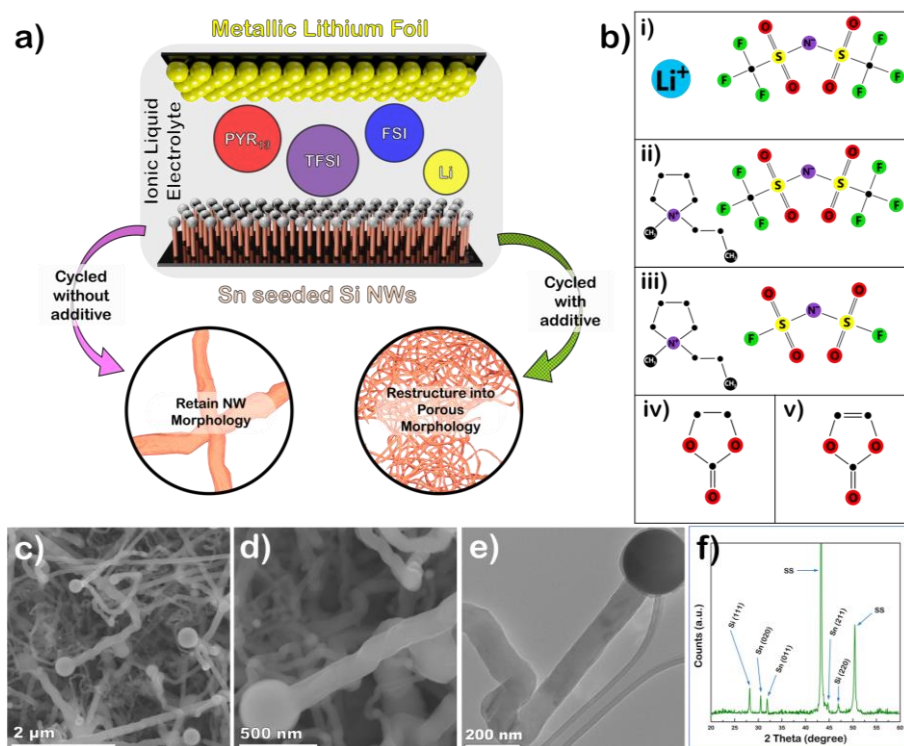


**Figure 1.** a) Schematic of Si NW half-cell testing and influence of electrolyte composition on structural evolution. b) Chemical structures of the electrolyte constituents: i) LiTFSI, ii) PYR<sub>13</sub>TFSI, iii) PYR<sub>13</sub>FSI, iv) EC, v) VC. c) Low and d) high magnification SEM images of the Sn-seeded Si NWs synthesized directly from SS current collects. e) TEM of a Si NW showing diameter of NW and spherical Sn seed. f) XRD taken of NW covered substrate where peaks for Si, Sn and the underlying SS can be seen.

The Sn seeded Si NWs were synthesized directly from the stainless-steel current collector eliminating the requirement for slurry processing of the electrodes and, additionally, ruling out interference from binders and conductive additives in our study (**Figure 1a**). The main electrolyte components are shown in **Figure 1b**. The wires are typically 100 nm in diameter with the Sn seed size of 400 nm as shown in SEM and TEM images **Figure 1 c-e**. The as-grown anodes used in this study had active mass loadings of approximately 0.2 mg/cm<sup>2</sup>. While the central focus of this study is on the impact of IL electrolyte formulations on Si NW stability and morphology during cycling, we acknowledge that the mass loadings investigated in this study are lower than that required for commercial systems. Nonetheless, practical mass loadings could potentially be achieved through greater morphological control (e.g. synthesizing longer Si NWs, thus maintaining the benefits afforded by the NW morphologies during cycling) and optimization of the current collector (e.g. by utilizing a 3D current collector with increased surface area or adopting a double-sided NW growth protocol). XRD revealed reflections consistent with cubic Si and tetragonal Sn (**Figure 1f**), with the remaining reflections from the stainless-steel current collector. Three different electrolyte compositions were investigated in this study, the pure IL and the IL with either the EC or the VC additive. The use of ternary (0.1LiTFSI-0.6PYR<sub>13</sub>FSI-0.3PYR<sub>13</sub>TFSI) and quaternary (0.1LiTFSI-0.6PYR<sub>13</sub>FSI-0.3PYR<sub>13</sub>TFSI + 5% EC or VC) electrolytes in this study aimed to combine the moderate viscosity, fast ion transport and thermal stability of PYR<sub>13</sub>FSI with the wide electrochemical and thermal stability afforded by PYR<sub>13</sub>TFSI.<sup>38</sup> A TFSI:FSI mole ratio of 2:3 was used on the basis of a previous study where it was determined to be the optimal ratio in terms of compromise between ion-transport, and thermal and rheological properties.<sup>38</sup> The addition of organic species does not compromise the safety of the battery as the small quantities ensure they are consumed within the first half cycle.<sup>48</sup>

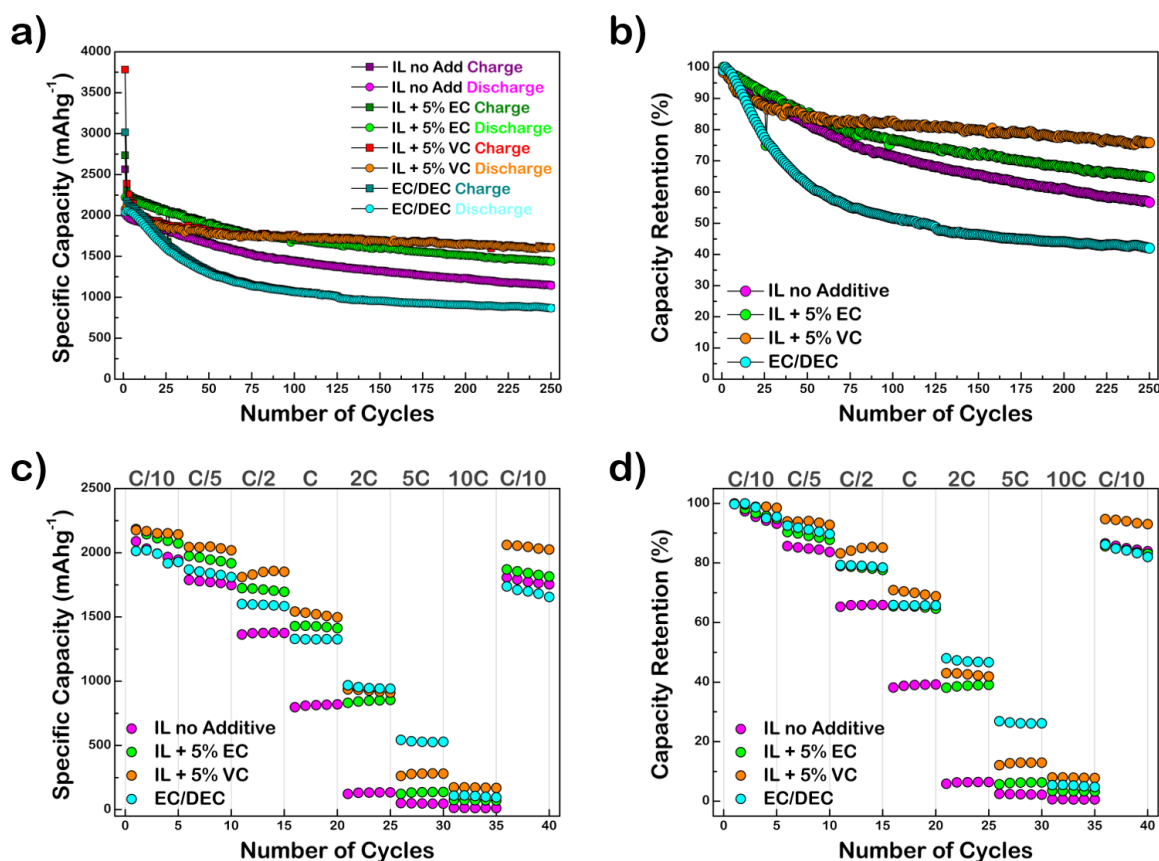


**Figure 2.** a) Charge and discharge capacities of the Si NWs over 250 cycles when cycled in each electrolyte composition. The material was cycled at a C/5 rate in a potential range of 0.01 – 1 V. b) Discharge capacity retention, plotted as a percentage, for each Si NW anode cycled in the IL electrolytes. c) Charge and discharge capacities at varying cycling rates of the Si NWs in each electrolyte composition and the associated d) Percentage capacity retention for the three electrolyte compositions tested.

The initial discharge (delithiation) capacities for each test were: 2016 mAhg<sup>-1</sup> (IL with no additive), 2220 mAhg<sup>-1</sup> (IL + 5% EC) and 2081 mAhg<sup>-1</sup> (IL + 5% VC) (**Figure 2a**). These gravimetric capacities translated to areal capacities in the range of: 0.44 – 0.40 mAh/cm<sup>2</sup>. After 250 cycles the anodes retained capacities of 1148 mAhg<sup>-1</sup> (no additive), 1443 mAhg<sup>-1</sup> (+ EC) and 1605 mAhg<sup>-1</sup> (+ VC) mAhg<sup>-1</sup>. These capacities corresponded to 57%, 65% and 77% retention, respectively (**Figure 2b**). **Figure 2** also compares the performance observed for the IL-based electrolytes to that of Si NWs cycled in an EC/DEC electrolyte in terms of gravimetric capacities and % capacity retention. The corresponding voltage profiles of the 1st, 10th, 25th,

50th, 100th, and 250th cycles for the four tests are presented in **Figure S1**. After 250 cycles, the Si NWs cycled in the EC/DEC electrolyte exhibited capacities of  $\sim 850 \text{ mAhg}^{-1}$  corresponding to 43% of the initial capacity retained. This is  $\sim 14\%$  lower than the performance in the pure ionic liquid and 34% lower than additive optimised IL. Ex-situ SEM analysis of the Si NWs after 100 cycles in the EC/DEC electrolyte (**Figure S2**) showed that the active material was fragmented into isolated regions that were tens of microns in size, which contrasts with a more interconnected and better anchored structure with similar cycles in the IL-based electrolytes (**Figure S3**). Improved coulombic efficiencies (CE) were evident in Si NWs cycled in the IL-based electrolytes versus the carbonate electrolyte (**Figure S4**). For the EC/DEC electrolyte, it took 100 cycles to reach 99% CE, a value that all three IL electrolytes had reached before the 50th cycle. As an unstable SEI, constantly under repair, is typically responsible for poor coulombic efficiency,<sup>49-50</sup> these results suggest the passivating layer formed by the decomposition of IL electrolytes is more robust and requires less repair on subsequent cycles and is reflected in the long-term stability for these electrodes.

The rate capability, evaluated by charging and discharging Si NW electrodes in each of the electrolytes for 5 cycles at rates of C/10, C/5, C/2, C, 2C, 5C, 10C and back to C/10, are shown in **Figure 2c** with the relative capacity retention as a percentage in **Figure 2d**. The ionic liquid with 5% VC performed best up to 1C, although at 2C and 5C the fully carbonate-based electrolyte performed better with capacities of  $530 \text{ mAhg}^{-1}$  at 5C. This suggests that while IL electrolytes can compete over long-term cycling, they still require improvement for high rate applications. At the fastest rate tested, 10C, while all electrodes exhibited poor capacities the highest was for IL + VC. One of the primary reasons for poorer performance at faster rates is due to low electrical conductivity and low rate of Li diffusion of Si.<sup>51</sup> When cycled again at C/10, the capacities returned to  $\sim 90\%$  of their initial values showing that the material is robust and remains electrically contacted to the current collector. The DCPs of the 2nd cycle for all

four tests are identical, showing that the two-step lithiation/delithiation of Si (**Figure S5**) is not significantly impacted by the electrolyte composition.

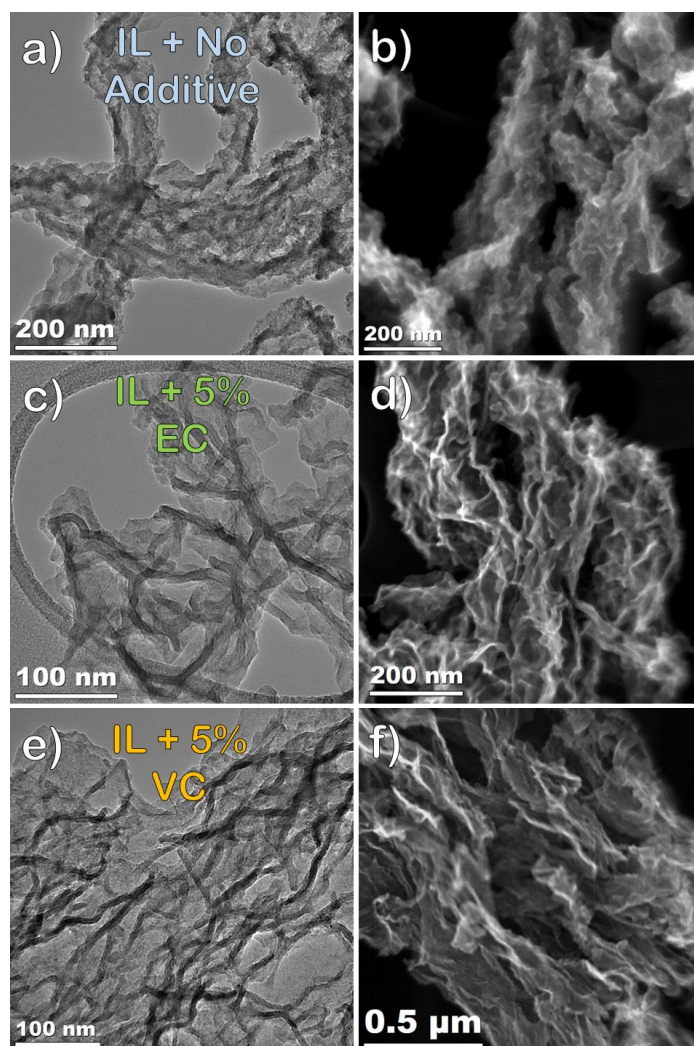


**Figure 3.** Ex-situ a) TEM and b) DFSTEM of the once-Si NW morphology after 100 cycles in 0.1LiTFSI-0.6PYR<sub>13</sub>FSI-0.3PYR<sub>13</sub>TFSI electrolyte. Ex-situ c) TEM and d) DFSTEM of the once-Si NW morphology after 100 cycles in 0.1LiTFSI-0.6PYR<sub>13</sub>FSI-0.3PYR<sub>13</sub>TFSI + 5% EC electrolyte. Ex-situ e) TEM and f) DFSTEM of the once-Si NW morphology after 100 cycles in 0.1LiTFSI-0.6PYR<sub>13</sub>FSI-0.3PYR<sub>13</sub>TFSI + 5% VC electrolyte.

SEM images of the active material with the SEI layer intact after 100 cycles revealed a thick coating across all visible areas (**Figure S6**). Following the chemical removal of the SEI, a notable difference between NWs cycled in the pure IL versus the NWs cycled in the presence

of the carbonate additives is observed. In the pure IL, while there was evidence of fusion between NWs, the morphology of the active material was less consistent, with the NW structures evident in a more textured form (**Figure 3a,b & Figure S3**). This suggests some NWs had stopped reversibly alloying contributing to the reduced capacities. The active material was composed of a network of nanometre-sized ligaments (**Figure 3c,d** for EC containing electrolyte and **Figure 3e,f** for VC containing electrolyte), resulting from a combination of pore formation and lithium assisted electrochemical welding over repeated lithiation/delithiation.<sup>4, 52-56</sup> The formation of this network has been previously observed to impart stability on the active material during long term cycling which coincides with an improved capacity retention observed here (for the additive containing ILs) in **Figure 3a**.<sup>14, 57</sup> Additional TEM images (**Figure S7**) of the restructured morphologies are presented in supporting information.

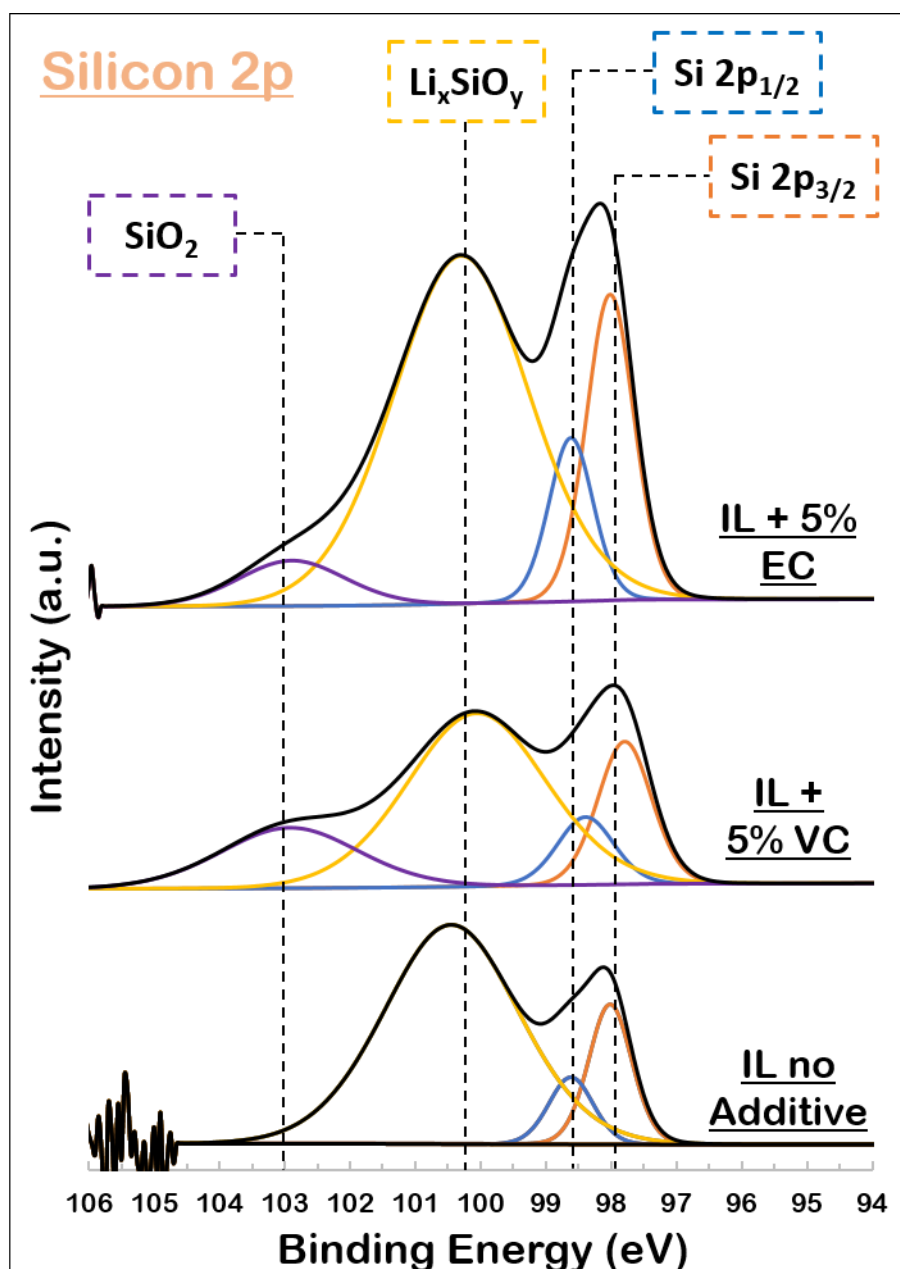


**Figure 4.** High resolution Si 2p spectra of the Si NWs after 100 cycles using each electrolyte additive. Prior to analysis the SEI layer was removed

The chemical composition of the cycled active material with the SEI removed was analyzed using XPS. The deconvoluted Si 2p spectrum, presented in **Figure 4**, indicates peaks for elemental Si and lithium silicates ( $\text{Li}_x\text{SiO}_y$ ) and silicon dioxide.<sup>51, 58-60</sup> The presented spectra are similar for all three electrolyte compositions, apart from an additional peak corresponding to  $\text{SiO}_2$  at approximately 103 eV for the additive containing electrolytes. This suggests a larger

portion of the elemental Si is consumed to form  $\text{Li}_x\text{SiO}_y$  in the pure IL compared to when the additives are used. This is evident from the more prominent  $\text{Li}_x\text{SiO}_y$  peak (100.5 eV) relative to the elemental Si peaks on the pure IL spectrum. Additionally, the fact that no peak exists for  $\text{SiO}_2$ , which is expected as the electrodes were exposed to air for the removal of the SEI, is further evidence that the surface of the additive free active material is composed of  $\text{Li}_x\text{SiO}_y$ . These silicate phases are known decomposition products for cycled Si electrodes.<sup>20-21, 30, 61-63</sup> Their presence in higher proportions at the surface of Si in the pure IL explains the poorer capacity retention of this electrode as their formation is irreversible. Conversely, the use of the additives helps create a more resilient SEI layer over the active material which is less likely to fracture and prevents unwanted consumption of Si. The more stable SEI layer appears to inhibit the formation of silicates, which, by forming chemically stable  $\text{SiO}_2$  layer on the surface of NWs at initial cycles, would block the surface toward further electrochemical processes.<sup>64</sup> This explains the improved cycling performance of the electrode material in the additive-containing electrolyte. Furthermore, the presence of the  $\text{Li}_x\text{SiO}_y$  phase at the surface of the additive free NWs may prevent the active material from partaking in lithium assisted electrochemical welding, thus inhibiting the formation of the mechanically robust interconnected porous network.<sup>30, 54</sup> It is noted that for all three spectra, no peaks exist at 105-106 eV, indicating the absence of  $\text{SiO}_x\text{F}_y$  species. This is an added benefit to using an IL based electrolyte salt (LiTFSI) over the traditional electrolyte salt,  $\text{LiPF}_6$ , which forms HF in the presence of trace amounts of moisture, which in turn reacts with  $\text{SiO}_2$  to form  $\text{SiO}_x\text{F}_y$ .<sup>65</sup> The stability and resistance of LiTFSI in forming HF has been attributed to a lower sensitivity to electrolysis.<sup>66</sup>

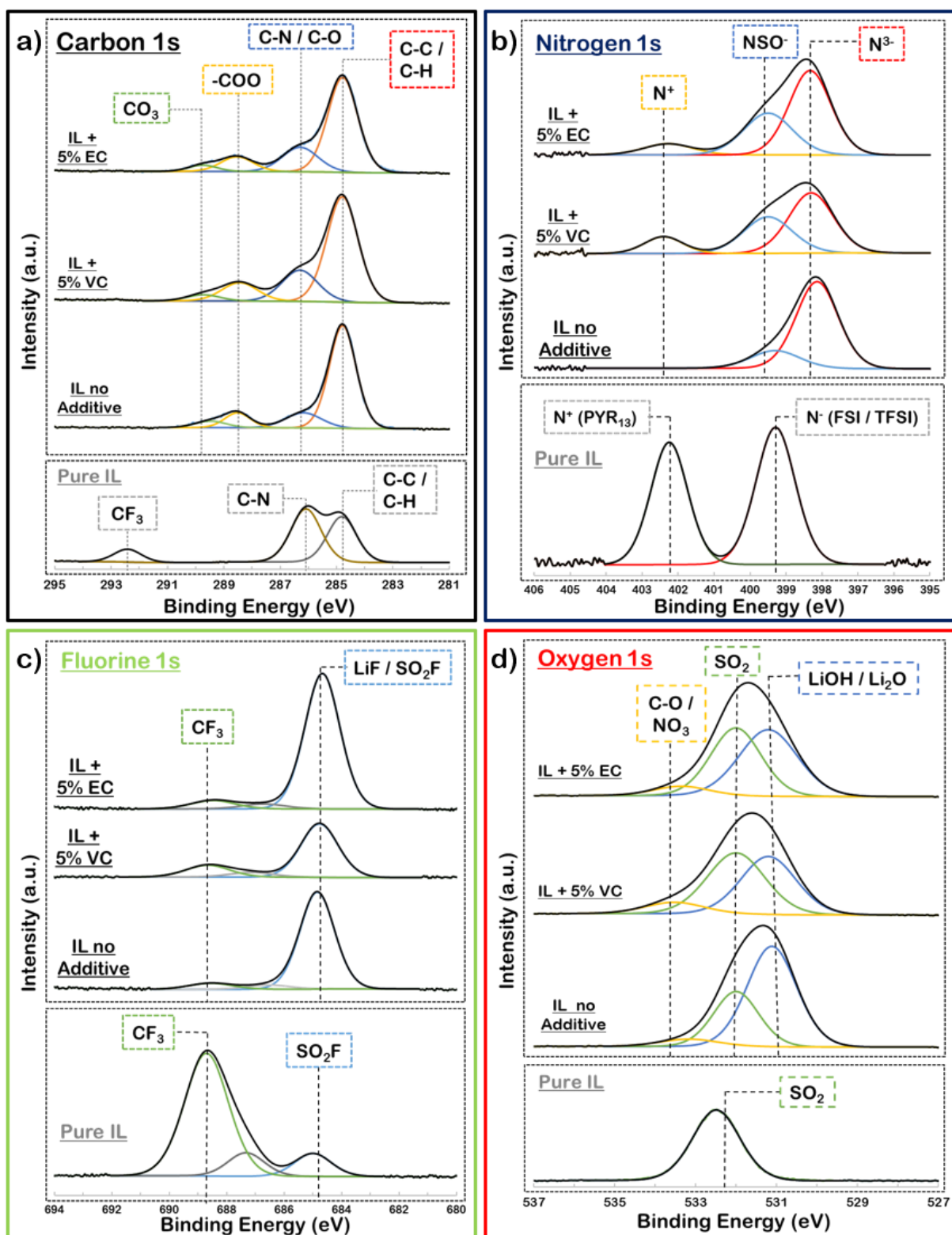


Figure 5. a) C 1s spectra of the SEI layer after 100 cycles using each additive as well as the XPS obtained for the IL directly. b) N 1s spectra of the Si NWs after 100 cycles using each additive as well as the XPS obtained for the IL directly. c) F 1s spectra of the Si NWs after 100 cycles using each additive as well as the XPS obtained for the IL directly. d) O 1s spectra of the Si NWs after 100 cycles using each additive as well as the XPS obtained for the IL directly.

The XPS C 1s spectra for the SEI of all three electrolyte compositions as well as the blank uncycled IL are presented in **Figure 5a**. Due to the low vapor pressures associated with ILs, it is difficult to completely remove all of the electrolyte, therefore XPS spectra of pure IL was used to identify residual IL on the ex-situ spectra.<sup>67</sup> Dimethylcarbonate was used to wash electrodes prior to analysis, as is standard in the field.<sup>30, 68</sup> In the C 1s, the most intense peak at 284.6 eV occurs due to hydrocarbon (CH) and the alkyl carbon (CC) species- degradation products from the PYR<sub>13</sub> ion and the carbonate additives. The peak at 286 eV corresponds to CN species from PYR<sub>13</sub> degradation and CO species due to breakdown of the carbonate-based electrolyte additives. As such, this peak is more prominent for the additive containing electrolytes due to the increased signal from carbonate degradation products in the SEI layer. The presence of the CO decomposition species is corroborated by a peak ~533 eV on the C 1s (**Figure 5d**).<sup>20</sup> The presence of CN species at the SEI surface is reciprocated in the N 1s spectra (**Figure 5b**) (403 eV). In the C 1s for the blank IL, a CF<sub>3</sub> peak at ~ 292.4 eV is due to the bonding environment of the TFSI anion. This is also reciprocated as a high intensity peak appearing at 688.7 eV on the F 1s spectra (**Figure 5c**) for the uncycled IL. This peak, albeit at a lower intensity, is present for all three electrolyte compositions after being subjected to 100 charge/discharge cycles.

On the N 1s XPS of the pure IL there are two peaks corresponding to the only two N environments of the uncycled electrolyte with the N<sup>+</sup> species (PYR<sub>13</sub><sup>+</sup>) appearing at approximately 402.2 eV and the N<sup>-</sup> species (TFSI<sup>-</sup>/FSI<sup>-</sup>) appearing at 399.3 eV, consistent with previously reported results.<sup>69</sup> The N 1s and F 1s confirm degradation of the IL components, in particular the anions, with additional species present for all three electrolyte compositions and disappearance of peaks present for the pure IL. For the N 1s, the peak corresponding to N<sup>+</sup> (401.5 eV) remains which may be due to residual PYR<sub>13</sub> in the SEI layer during XPS analysis, however the peak most likely corresponds to a nitrate species due to the indication of an NO<sub>3</sub>

species on the O 1s at approximately 533.4 eV (**Figure 5d**). The most intense peak on the F 1s spectra is that for the LiF species (684.7 eV) which is attributed to the reaction between Li and the reduced IL anions.<sup>36, 70</sup> Furthermore, the peak for LiF, the presence of which on the surface of NWs would lead to sluggish Li<sup>+</sup> transport kinetics and consequent capacity fading due to its high resistivity, is less pronounced in the VC-added IL-based electrolyte.<sup>71</sup> During lithiation, the FSI anion reduces to a SO<sub>2</sub>F<sup>•</sup> radical as an initial degradation product before losing an F<sup>•</sup> that forms LiF species present in the SEI,<sup>70, 72</sup> while also forming an SO<sub>2</sub> containing species.<sup>35-</sup><sup>36</sup> The presence of a SO<sub>2</sub> (SO<sub>2</sub><sup>•</sup> or –SO<sub>2</sub>) environment is confirmed on the S 2p spectrum at approximately 168 eV (**Figure S8**). TFSI, a more robust ion, is initially reduced to a N(SO<sub>2</sub>CF<sub>3</sub>)<sub>2</sub><sup>•</sup> radical before reacting again.<sup>67, 73</sup> The most probable route, involves the breaking of one of the S-N bonds, forming <sup>•</sup>NSO<sub>3</sub>CF<sub>3</sub> and SO<sub>2</sub>CF<sub>3</sub><sup>•</sup>.<sup>74</sup> Another potential route involves cleavage of the reduced C-S bond with the resulting ions predicted to undergo further reductive decomposition, yielding species such as NSO, CF<sub>3</sub>, and SO<sub>2</sub>, which form insoluble components in the SEI with Li.<sup>75-77</sup> The NSO species is present in the SEI layer and confirmed on the N 1s spectra at 400 eV. Additionally, a peak at ~398 eV likely corresponds to a nitride (N<sup>3-</sup>) species on the N 1s spectra (Figure 5b).<sup>68, 78-79</sup> NSO, which is electronically insulating, but ion-conductive, is more pronounced in VC- or EC-added IL electrolytes versus the pure IL electrolyte. This is significant as NSO protects the NW surface against the electrolyte, while providing excellent Li<sup>+</sup> diffusion kinetics.<sup>80</sup>

While most of the decomposition products can be related to the FSI and TFSI, the PYR<sub>13</sub> cation also contributes to the SEI composition. The N 1s spectra suggests a breakdown of the PYR<sub>13</sub> cation which then provides the H<sup>+</sup> for the formation of the LiOH species present in the SEI appearing on the O 1s spectra at ~531 eV.<sup>36, 70</sup> However, this is the same region where LiO<sub>2</sub> is also expected. Additionally, LiOH/LiO<sub>2</sub>, SO<sub>2</sub> and NO<sub>3</sub> containing species are highlighted as decomposition products, for all three electrolyte compositions after 100 cycles

in the O 1s spectra. The deconvoluted S 2p spectrum clearly shows the presence of SO<sub>2</sub> species in the SEI for all three tests and, as discussed, is a degradation product of both the FSI and TFSI anions.<sup>81</sup> Additionally, the SO<sub>2</sub> species likely breaks down further to form sulphate, sulphite and sulphide species which are accounted for on the S 2p spectrum.<sup>70, 82</sup> These peaks are all consistent for the three electrolyte compositions as the presence of S in the SEI is exclusively due to degradation of the IL components.

## **Conclusions**

High reversible capacities and improved long-term cycling stability were observed for Si NW anodes when cycled in safer, flame retardant IL electrolytes incorporating a small sacrificial amount of carbonate additives. This improved Li-ion battery performance over conventional carbonate-based electrolytes resulted from a more robust SEI that required less repair upon each cycle. VC containing IL electrolytes showed a 20% improvement over the pure IL electrolyte and a 34% improvement over the conventional carbonate-based electrolyte. It was discovered, through ex-situ XPS and electron microscopy, that these additives helped form a more resilient SEI layer which inhibited the irreversible decomposition of elemental Si to lithium silicates at the surface of NWs. This facilitated the complete restructuring of the active material to a fused interconnected network, which bestowed improved capacity retention on the material. This study highlights the potential of ILs as safe, higher performance alternatives to carbonate-based electrolytes for future Li-ion battery applications.

## **Associated Content**

### **Supporting Information**

The Supporting Information is available free of charge on the ACS Publications website at DOI:

## Acknowledgements

This work was supported by Science Foundation Ireland (SFI) under the Principal Investigator Program under Contract Nos. 16/IA/4629, 11-PI-1148 and under Grant SFI 16/M-ERA/3419. This project has received funding from the European Union's Horizon 2020 research and innovation programme under grant agreement No 814464 (Si-DRIVE project). K.S. thanks the Irish Research Council for funding through the Government of Ireland Postgraduate Scheme. H.G. acknowledges SIRG under grant 18/SIRG/5484 and Enterprise Ireland under Contract No. CF20144014.

## Notes

The authors declare no competing financial interest

## References

1. Tarascon, J. M.; Armand, M., Issues and challenges facing rechargeable lithium batteries. *Nature* **2001**, *414* (6861), 359-367.
2. Armand, M.; Tarascon, J. M., Building better batteries. *Nature* **2008**, *451* (7179), 652-657.
3. Nishi, Y., Lithium ion secondary batteries; past 10 years and the future. *Journal of Power Sources* **2001**, *100* (1), 101-106.
4. Kennedy, T.; Brandon, M.; Ryan, K. M., Advances in the Application of Silicon and Germanium Nanowires for High-Performance Lithium-Ion Batteries. *Advanced Materials* **2016**, *28* (27), 5696-5704.
5. Winter, M.; Besenhard, J. O., Electrochemical lithiation of tin and tin-based intermetallics and composites. *Electrochimica Acta* **1999**, *45* (1-2), 31-50.
6. Zamfir, M. R.; Nguyen, H. T.; Moyon, E.; Lee, Y. H.; Pribat, D., Silicon nanowires for Li-based battery anodes: a review. *Journal of Materials Chemistry A* **2013**, *1* (34), 9566-9586.
7. Kasavajjula, U.; Wang, C.; Appleby, A. J., Nano- and bulk-silicon-based insertion anodes for lithium-ion secondary cells. *Journal of Power Sources* **2007**, *163* (2), 1003-1039.
8. Liu, X. H.; Zhong, L.; Huang, S.; Mao, S. X.; Zhu, T.; Huang, J. Y., Size-Dependent Fracture of Silicon Nanoparticles During Lithiation. *ACS Nano* **2012**, *6* (2), 1522-1531.
9. Chan, C. K.; Peng, H.; Liu, G.; McIlwrath, K.; Zhang, X. F.; Huggins, R. A.; Cui, Y., High-performance lithium battery anodes using silicon nanowires. *Nature nanotechnology* **2008**, *3* (1), 31-35.
10. Chan, C. K.; Patel, R. N.; O'Connell, M. J.; Korgel, B. A.; Cui, Y., Solution-Grown Silicon Nanowires for Lithium-Ion Battery Anodes. *ACS Nano* **2010**, *4* (3), 1443-1450.
11. Su, X.; Wu, Q.; Li, J.; Xiao, X.; Lott, A.; Lu, W.; Sheldon, B. W.; Wu, J., Silicon-Based Nanomaterials for Lithium-Ion Batteries: A Review. *Advanced Energy Materials* **2014**, *4* (1), 1300882-n/a.
12. Bogart, T. D.; Chockla, A. M.; Korgel, B. A., High capacity lithium ion battery anodes of silicon and germanium. *Current Opinion in Chemical Engineering* **2013**, *2* (3), 286-293.
13. Cho, J.-H.; Picraux, S. T., Enhanced Lithium Ion Battery Cycling of Silicon Nanowire Anodes by Template Growth to Eliminate Silicon Underlayer Islands. *Nano Letters* **2013**, *13* (11), 5740-5747.
14. Kennedy, T.; Mullane, E.; Geaney, H.; Osiak, M.; O'Dwyer, C.; Ryan, K. M., High-performance germanium nanowire-based lithium-ion battery anodes extending over 1000

cycles through in situ formation of a continuous porous network. *Nano letters* **2014**, *14* (2), 716-723.

15. Chockla, A. M.; Harris, J. T.; Akhavan, V. A.; Bogart, T. D.; Holmberg, V. C.; Steinhagen, C.; Mullins, C. B.; Stevenson, K. J.; Korgel, B. A., Silicon Nanowire Fabric as a Lithium Ion Battery Electrode Material. *Journal of the American Chemical Society* **2011**, *133* (51), 20914-20921.

16. Wu, H.; Chan, G.; Choi, J. W.; Ryu, I.; Yao, Y.; McDowell, M. T.; Lee, S. W.; Jackson, A.; Yang, Y.; Hu, L.; Cui, Y., Stable cycling of double-walled silicon nanotube battery anodes through solid-electrolyte interphase control. *Nature Nanotechnology* **2012**, *7*, 310.

17. Xie, J.; Cao, G. S.; Zhao, X. B., Electrochemical performances of Si-coated MCMB as anode material in lithium-ion cells. *Materials Chemistry and Physics* **2004**, *88* (2), 295-299.

18. Landi, B. J.; Cress, C. D.; Raffaele, R. P., High energy density lithium-ion batteries with carbon nanotube anodes. *Journal of Materials Research* **2011**, *25* (8), 1636-1644.

19. Wu, H.; Yu, G.; Pan, L.; Liu, N.; McDowell, M. T.; Bao, Z.; Cui, Y., Stable Li-ion battery anodes by in-situ polymerization of conducting hydrogel to conformally coat silicon nanoparticles. *Nature Communications* **2013**, *4*, ncomms2941.

20. Radvanyi, E.; De Vito, E.; Porcher, W.; Larbi, S. J. S., An XPS/AES comparative study of the surface behaviour of nano-silicon anodes for Li-ion batteries. *Journal of Analytical Atomic Spectrometry* **2014**, *29* (6), 1120-1131.

21. Nie, M.; Abraham, D. P.; Chen, Y.; Bose, A.; Lucht, B. L., Silicon solid electrolyte interphase (SEI) of lithium ion battery characterized by microscopy and spectroscopy. *The Journal of Physical Chemistry C* **2013**, *117* (26), 13403-13412.

22. Stokes, K.; Boonen, W.; Geaney, H.; Kennedy, T.; Borsa, D.; Ryan, K. M., Tunable Core-Shell Nanowire Active Material for High Capacity Li-Ion Battery Anodes Comprised of PECVD Deposited aSi on Directly Grown Ge Nanowires. *ACS Applied Materials & Interfaces* **2019**, *11* (21), 19372-19380.

23. Xu, Y.; Stetson, C.; Wood, K.; Sivonxay, E.; Jiang, C.; Teeter, G.; Pylypenko, S.; Han, S.-D.; Persson, K. A.; Burrell, A.; Zakutayev, A., Mechanical Properties and Chemical Reactivity of  $\text{Li}_x\text{SiO}_y$  Thin Films. *ACS Applied Materials & Interfaces* **2018**, *10* (44), 38558-38564.

24. Yom, J. H.; Hwang, S. W.; Cho, S. M.; Yoon, W. Y., Improvement of irreversible behavior of SiO anodes for lithium ion batteries by a solid state reaction at high temperature. *Journal of Power Sources* **2016**, *311*, 159-166.

25. Zhang, S. S., A review on electrolyte additives for lithium-ion batteries. *Journal of Power Sources* **2006**, *162* (2), 1379-1394.

26. Etacheri, V.; Haik, O.; Goffer, Y.; Roberts, G. A.; Stefan, I. C.; Fasching, R.; Aurbach, D., Effect of Fluoroethylene Carbonate (FEC) on the Performance and Surface Chemistry of Si-Nanowire Li-Ion Battery Anodes. *Langmuir* **2012**, *28* (1), 965-976.

27. El Ouatani, L.; Dedryvère, R.; Siret, C.; Biensan, P.; Reynaud, S.; Iratçabal, P.; Gonbeau, D., The Effect of Vinylene Carbonate Additive on Surface Film Formation on Both Electrodes in Li-Ion Batteries. *Journal of The Electrochemical Society* **2009**, *156* (2), A103-A113.

28. Dalavi, S.; Guduru, P.; Lucht, B. L., Performance Enhancing Electrolyte Additives for Lithium Ion Batteries with Silicon Anodes. *Journal of The Electrochemical Society* **2012**, *159* (5), A642-A646.

29. Jin, Y.; Kneusels, N.-J. H.; Marbella, L. E.; Castillo-Martínez, E.; Magusin, P. C. M. M.; Weatherup, R. S.; Jónsson, E.; Liu, T.; Paul, S.; Grey, C. P., Understanding Fluoroethylene Carbonate and Vinylene Carbonate Based Electrolytes for Si Anodes in Lithium Ion Batteries with NMR Spectroscopy. *Journal of the American Chemical Society* **2018**, *140* (31), 9854-9867.

30. Kennedy, T.; Brandon, M.; Laffir, F.; Ryan, K. M., Understanding the influence of electrolyte additives on the electrochemical performance and morphology evolution of silicon nanowire based lithium-ion battery anodes. *Journal of Power Sources* **2017**, *359*, 601-610.
31. Barchasz, C.; Leprêtre, J.-C.; Patoux, S.; Alloin, F., Revisiting TEGDME/DIOX Binary Electrolytes for Lithium/Sulfur Batteries: Importance of Solvation Ability and Additives. *Journal of The Electrochemical Society* **2013**, *160* (3), A430-A436.
32. Armand, M.; Endres, F.; MacFarlane, D. R.; Ohno, H.; Scrosati, B., Ionic-liquid materials for the electrochemical challenges of the future. *Nature Materials* **2009**, *8*, 621.
33. Moreno, M.; Simonetti, E.; Appetecchi, G. B.; Carewska, M.; Montanino, M.; Kim, G.-T.; Loeffler, N.; Passerini, S., Ionic Liquid Electrolytes for Safer Lithium Batteries: I. Investigation around Optimal Formulation. *Journal of The Electrochemical Society* **2017**, *164* (1), A6026-A6031.
34. Zhou, Q.; Boyle, P. D.; Malpezzi, L.; Mele, A.; Shin, J.-H.; Passerini, S.; Henderson, W. A., Phase Behavior of Ionic Liquid–LiX Mixtures: Pyrrolidinium Cations and TFSI–Anions – Linking Structure to Transport Properties. *Chemistry of Materials* **2011**, *23* (19), 4331-4337.
35. Howlett, P. C.; MacFarlane, D. R.; Hollenkamp, A. F., High Lithium Metal Cycling Efficiency in a Room-Temperature Ionic Liquid. *Electrochemical and Solid-State Letters* **2004**, *7* (5), A97-A101.
36. Howlett, P. C.; Brack, N.; Hollenkamp, A. F.; Forsyth, M.; MacFarlane, D. R., Characterization of the Lithium Surface in N-Methyl-N-alkylpyrrolidinium Bis(trifluoromethanesulfonyl)amide Room-Temperature Ionic Liquid Electrolytes. *Journal of The Electrochemical Society* **2006**, *153* (3), A595-A606.
37. Paillard, E.; Zhou, Q.; Henderson, W. A.; Appetecchi, G. B.; Montanino, M.; Passerini, S., Electrochemical and Physicochemical Properties of PY14FSI -Based Electrolytes with LiFSI. *Journal of The Electrochemical Society* **2009**, *156* (11), A891-A895.
38. Kim, G.-T.; Kennedy, T.; Brandon, M.; Geaney, H.; Ryan, K. M.; Passerini, S.; Appetecchi, G. B., Behavior of Germanium and Silicon Nanowire Anodes with Ionic Liquid Electrolytes. *ACS Nano* **2017**, *11* (6), 5933-5943.
39. Baranchugov, V.; Markevich, E.; Pollak, E.; Salitra, G.; Aurbach, D., Amorphous silicon thin films as a high capacity anodes for Li-ion batteries in ionic liquid electrolytes. *Electrochemistry Communications* **2007**, *9* (4), 796-800.
40. Chakrapani, V.; Rusli, F.; Filler, M. A.; Kohl, P. A., Quaternary Ammonium Ionic Liquid Electrolyte for a Silicon Nanowire-Based Lithium Ion Battery. *The Journal of Physical Chemistry C* **2011**, *115* (44), 22048-22053.
41. Ivanov, S.; Vlaic, C. A.; Du, S.; Wang, D.; Schaaf, P.; Bund, A., Electrochemical performance of nanoporous Si as anode for lithium ion batteries in alkyl carbonate and ionic liquid-based electrolytes. *Journal of Applied Electrochemistry* **2014**, *44* (1), 159-168.
42. Shimizu, M.; Usui, H.; Matsumoto, K.; Nokami, T.; Itoh, T.; Sakaguchi, H., Effect of Cation Structure of Ionic Liquids on Anode Properties of Si Electrodes for LIB. *Journal of The Electrochemical Society* **2014**, *161* (12), A1765-A1771.
43. Yabuuchi, N.; Shimomura, K.; Shimbe, Y.; Ozeki, T.; Son, J.-Y.; Oji, H.; Katayama, Y.; Miura, T.; Komaba, S., Graphite-Silicon-Polyacrylate Negative Electrodes in Ionic Liquid Electrolyte for Safer Rechargeable Li-Ion Batteries. *Advanced Energy Materials* **2011**, *1* (5), 759-765.
44. Seddon, K. R., A taste of the future. *Nature Materials* **2003**, *2*, 363.
45. Physical Properties of Ionic Liquids: Database and Evaluation. *Journal of Physical and Chemical Reference Data* **2006**, *35* (4), 1475-1517.
46. Wasserscheid, P., Volatile times for ionic liquids. *Nature* **2006**, *439*, 797.

47. Lewandowski, A.; Świdarska-Mocek, A., Ionic liquids as electrolytes for Li-ion batteries—An overview of electrochemical studies. *Journal of Power Sources* **2009**, *194* (2), 601-609.
48. Montanino, M.; Moreno, M.; Carewska, M.; Maresca, G.; Simonetti, E.; Lo Presti, R.; Alessandrini, F.; Appetecchi, G. B., Mixed organic compound-ionic liquid electrolytes for lithium battery electrolyte systems. *Journal of Power Sources* **2014**, *269*, 608-615.
49. An, S. J.; Li, J.; Daniel, C.; Mohanty, D.; Nagpure, S.; Wood III, D. L., The state of understanding of the lithium-ion-battery graphite solid electrolyte interphase (SEI) and its relationship to formation cycling. *Carbon* **2016**, *105*, 52-76.
50. Etacheri, V.; Marom, R.; Elazari, R.; Salitra, G.; Aurbach, D., Challenges in the development of advanced Li-ion batteries: a review. *Energy & Environmental Science* **2011**, *4* (9), 3243-3262.
51. Philippe, B.; Dedryvère, R.; Gorgoi, M.; Rensmo, H.; Gonbeau, D.; Edström, K., Improved Performances of Nanosilicon Electrodes Using the Salt LiFSI: A Photoelectron Spectroscopy Study. *Journal of the American Chemical Society* **2013**, *135* (26), 9829-9842.
52. Geaney, H.; Bree, G.; Stokes, K.; Collins, G. A.; Aminu, I. S.; Kennedy, T.; Ryan, K. M., Enhancing the performance of germanium nanowire anodes for Li-ion batteries by direct growth on textured copper. *Chemical Communications* **2019**, *55* (54), 7780-7783.
53. Stokes, K.; Geaney, H.; Flynn, G.; Sheehan, M.; Kennedy, T.; Ryan, K. M., Direct Synthesis of Alloyed Si<sub>1-x</sub>Ge<sub>x</sub> Nanowires for Performance-Tunable Lithium Ion Battery Anodes. *ACS Nano* **2017**, *11* (10), 10088-10096.
54. Karki, K.; Epstein, E.; Cho, J.-H.; Jia, Z.; Li, T.; Picraux, S. T.; Wang, C.; Cumings, J., Lithium-Assisted Electrochemical Welding in Silicon Nanowire Battery Electrodes. *Nano Letters* **2012**, *12* (3), 1392-1397.
55. Choi, J. W.; McDonough, J.; Jeong, S.; Yoo, J. S.; Chan, C. K.; Cui, Y., Stepwise Nanopore Evolution in One-Dimensional Nanostructures. *Nano Letters* **2010**, *10* (4), 1409-1413.
56. Stokes, K.; Geaney, H.; Sheehan, M.; Borsa, D.; Ryan, K. M., Copper Silicide Nanowires as Hosts for Amorphous Si Deposition as a Route to Produce High Capacity Lithium-Ion Battery Anodes. *Nano Letters* **2019**, *19* (12), 8829-8835.
57. Stokes, K.; Flynn, G.; Geaney, H.; Bree, G.; Ryan, K. M., Axial Si–Ge Heterostructure Nanowires as Lithium-Ion Battery Anodes. *Nano Letters* **2018**, *18* (9), 5569-5575.
58. Ulgut, B.; Suzer, S., XPS Studies of SiO<sub>2</sub>/Si System under External Bias. *The Journal of Physical Chemistry B* **2003**, *107* (13), 2939-2943.
59. Koshizaki, N.; Umehara, H.; Oyama, T., XPS characterization and optical properties of Si/SiO<sub>2</sub>, Si/Al<sub>2</sub>O<sub>3</sub> and Si/MgO co-sputtered films. *Thin Solid Films* **1998**, *325* (1), 130-136.
60. Philippe, B.; Dedryvère, R.; Gorgoi, M.; Rensmo, H.; Gonbeau, D.; Edström, K., Role of the LiPF<sub>6</sub> Salt for the Long-Term Stability of Silicon Electrodes in Li-Ion Batteries – A Photoelectron Spectroscopy Study. *Chemistry of Materials* **2013**, *25* (3), 394-404.
61. Schroder, K.; Alvarado, J.; Yersak, T. A.; Li, J.; Dudney, N.; Webb, L. J.; Meng, Y. S.; Stevenson, K. J., The Effect of Fluoroethylene Carbonate as an Additive on the Solid Electrolyte Interphase on Silicon Lithium-Ion Electrodes. *Chemistry of Materials* **2015**, *27* (16), 5531-5542.
62. Kim, J. S.; Byun, D.; Lee, J. K., Electrochemical characteristics of amorphous silicon thin film electrode with fluoroethylene carbonate additive. *Current Applied Physics* **2014**, *14* (4), 596-602.
63. Philippe, B.; Hahlin, M.; Edström, K.; Gustafsson, T.; Siegbahn, H.; Rensmo, H., Photoelectron spectroscopy for lithium battery interface studies. *Journal of The Electrochemical Society* **2016**, *163* (2), A178-A191.

64. Song, J.-W.; Nguyen, C. C.; Song, S.-W., Stabilized cycling performance of silicon oxide anode in ionic liquid electrolyte for rechargeable lithium batteries. *RSC Advances* **2012**, 2 (5), 2003-2009.
65. Aurbach, D.; Markovsky, B.; Shechter, A.; Ein-Eli, Y.; Cohen, H., A Comparative Study of Synthetic Graphite and Li Electrodes in Electrolyte Solutions Based on Ethylene Carbonate-Dimethyl Carbonate Mixtures. *Journal of The Electrochemical Society* **1996**, 143 (12), 3809-3820.
66. Han, H.-B.; Zhou, S.-S.; Zhang, D.-J.; Feng, S.-W.; Li, L.-F.; Liu, K.; Feng, W.-F.; Nie, J.; Li, H.; Huang, X.-J.; Armand, M.; Zhou, Z.-B., Lithium bis(fluorosulfonyl)imide (LiFSI) as conducting salt for nonaqueous liquid electrolytes for lithium-ion batteries: Physicochemical and electrochemical properties. *Journal of Power Sources* **2011**, 196 (7), 3623-3632.
67. Dupré, N.; Moreau, P.; De Vito, E.; Quazuguel, L.; Boniface, M.; Kren, H.; Bayle-Guillemaud, P.; Guyomard, D., Carbonate and Ionic Liquid Mixes as Electrolytes To Modify Interphases and Improve Cell Safety in Silicon-Based Li-Ion Batteries. *Chemistry of Materials* **2017**, 29 (19), 8132-8146.
68. Nguyen, C. C.; Song, S.-W., Characterization of SEI layer formed on high performance Si-Cu anode in ionic liquid battery electrolyte. *Electrochemistry Communications* **2010**, 12 (11), 1593-1595.
69. Men, S.; Hurisso, B. B.; Lovelock, K. R. J.; Licence, P., Does the influence of substituents impact upon the surface composition of pyrrolidinium-based ionic liquids? An angle resolved XPS study. *Physical Chemistry Chemical Physics* **2012**, 14 (15), 5229-5238.
70. Budi, A.; Basile, A.; Opletal, G.; Hollenkamp, A. F.; Best, A. S.; Rees, R. J.; Bhatt, A. I.; O'Mullane, A. P.; Russo, S. P., Study of the Initial Stage of Solid Electrolyte Interphase Formation upon Chemical Reaction of Lithium Metal and N-Methyl-N-Propyl-Pyrrolidinium-Bis(Fluorosulfonyl)Imide. *The Journal of Physical Chemistry C* **2012**, 116 (37), 19789-19797.
71. Tu, W.; Xia, P.; Zheng, X.; Ye, C.; Xu, M.; Li, W., Insight into the interaction between layered lithium-rich oxide and additive-containing electrolyte. *Journal of Power Sources* **2017**, 341, 348-356.
72. Herlem, M.; Mathieu, C.; Herlem, D., About the reaction between asphaltenes and fluorosulfuric acid. *Fuel* **2004**, 83 (11), 1665-1668.
73. Yildirim, H.; Haskins, J. B.; Bauschlicher, C. W.; Lawson, J. W., Decomposition of Ionic Liquids at Lithium Interfaces. 1. Ab Initio Molecular Dynamics Simulations. *The Journal of Physical Chemistry C* **2017**, 121 (51), 28214-28234.
74. Howlett Patrick, C.; Izgorodina Ekaterina, I.; Forsyth, M.; MacFarlane Douglas, R., Electrochemistry at Negative Potentials in Bis(trifluoromethanesulfonyl)amide Ionic Liquids. In *Zeitschrift für Physikalische Chemie*, 2006; Vol. 220, p 1483.
75. Shkrob, I. A.; Marin, T. W.; Zhu, Y.; Abraham, D. P., Why Bis(fluorosulfonyl)imide Is a "Magic Anion" for Electrochemistry. *The Journal of Physical Chemistry C* **2014**, 118 (34), 19661-19671.
76. Markevich, E.; Sharabi, R.; Borgel, V.; Gottlieb, H.; Salitra, G.; Aurbach, D.; Semrau, G.; Schmidt, M. A., In situ FTIR study of the decomposition of N-butyl-N-methylpyrrolidinium bis(trifluoromethanesulfonyl)amide ionic liquid during cathodic polarization of lithium and graphite electrodes. *Electrochimica Acta* **2010**, 55 (8), 2687-2696.
77. Basile, A.; Hollenkamp, A. F.; Bhatt, A. I.; O'Mullane, A. P., Extensive charge-discharge cycling of lithium metal electrodes achieved using ionic liquid electrolytes. *Electrochemistry Communications* **2013**, 27, 69-72.
78. Ishiyama, S.; Baba, Y.; Fujii, R.; Nakamura, M.; Imahori, Y., Synthesis of lithium nitride for neutron production target of BNCT by in situ lithium deposition and ion implantation. *Nuclear Instruments and Methods in Physics Research Section B: Beam Interactions with Materials and Atoms* **2012**, 293, 42-47.

79. D., B., Handbook of X-ray Photoelectron Spectroscopy C. D. Wanger, W. M. Riggs, L. E. Davis, J. F. Moulder and G. E. Muilenberg Perkin-Elmer Corp., Physical Electronics Division, Eden Prairie, Minnesota, USA, 1979. 190 pp. \$195. *Surface and Interface Analysis* **1981**, 3 (4), v-v.
80. Qin, B.; Jeong, S.; Zhang, H.; Ulissi, U.; Vieira Carvalho, D.; Varzi, A.; Passerini, S., Enabling Reversible (De)Lithiation of Aluminum by using Bis(fluorosulfonyl)imide-Based Electrolytes. *ChemSusChem* **2019**, 12 (1), 208-212.
81. Piper, D. M.; Evans, T.; Leung, K.; Watkins, T.; Olson, J.; Kim, S. C.; Han, S. S.; Bhat, V.; Oh, K. H.; Buttry, D. A.; Lee, S.-H., Stable silicon-ionic liquid interface for next-generation lithium-ion batteries. *Nature Communications* **2015**, 6, 6230.
82. Xiong, S.; Xie, K.; Blomberg, E.; Jacobsson, P.; Matic, A., Analysis of the solid electrolyte interphase formed with an ionic liquid electrolyte for lithium-sulfur batteries. *Journal of Power Sources* **2014**, 252, 150-155.